Ultrafast electron-lattice coupling in cobalt films probed by nanoscale extreme ultraviolet transient gratings

G. Kurdi,[1] D. Fainozzi,[1,2] L. Foglia,[1] N. Khatu,[1,3] S. Laterza,[1] R. Mincigrucci,[1] E. Paltanin,[1] J. S. Pelli-Cresi,[1] B. Wehinger,[3,4] S. Bonetti,[3] C. Masciovecchio,[1] and F. Bencivenga[1,*]

[1]*Elettra-Sincrotrone Trieste, S.S. 15 km 163,5 in AREA Science Park, 34149 Basovizza, Italy*

[2]*Institute of Applied Physics, University of Bern, Bern, Switzerland*

[3]*Department of Molecular Sciences and Nanosystems, Ca'Foscari University of Venice, Venice, Italy*

[4]*European Synchrotron Radiation Facility, 71 avenue des Martyrs, 38043 Grenoble, France*

(Received 16 December 2025; revised 16 April 2026; accepted 9 June 2026; published 6 July 2026)

Extreme ultraviolet transient gratings (EUV TG) are a recently developed tool, originally conceived for probing thermoelastic dynamics and more recently extended to magnetic dynamics through the use of core-resonant EUV probing. Resonant EUV probes also enable probing the ultrafast electronic response. Here we report on the observation of a prominent electronic response observed from a cobalt film in transmission geometry, when the photon energy is tuned to the $M_{2,3}$ edge of the sample (59.6 eV). The observed dynamics is consistent with a population grating of electronic excitations, which represents the initial step of the EUV TG excitation process and, in a subpicosecond timescale, decays through electron-lattice coupling. On longer timescales, the resulting lattice excitation grating drives the thermoelastic response, regularly observed in EUV TG experiments and featured by acoustic oscillations that modulate the time decay of the lattice temperature grating. The ultrafast electronic relaxation dynamics is no longer observed when the photon energy is largely off resonance, indicating the need for a resonant EUV probe to detect it. While a photon energy scan in a narrow range around the edge does not show sizable changes in the electron-lattice relaxation dynamics, the showcased capability of imposing a nanoscale spatial modulation of the excitation pulse enables the possibility to use a variable EUV TG periodicity to study electronic relaxation dynamics at the nanoscale.

DOI: 10.1103/j1rk-j6rt

I. INTRODUCTION

The dynamics of charge, spin and temperature relaxations at the nanoscale are fundamental aspects of modern research, which often requires ultrafast time resolution for being experimentally studied. While ultrafast laser pulses can achieve such a time resolution, nanometer length scales are beyond the range of optical wavelengths, unless *ad hoc* nanopatterning of the samples is used [1–3]. An alternative approach to achieve nanoscale sensitivity is to use ultrafast pulses at suboptical wavelengths, that is, the extreme ultraviolet (EUV) and x-ray ranges. In this context, the recent development of the EUV transient grating (TG) approach enables selecting specific spatial scales in the tens of a nanometer range [4,5].

EUV TG with EUV probes was initially developed for probing nanoscale thermoelastic dynamics of both bulk and surface nature [4,6–8], and recently extended to magnetic dynamics through the use of resonant EUV probes [9–12]. While the use of nonresonant EUV probes has demonstrated high sensitivity to the thermoelastic dynamics, but almost no signatures of any electronic response, resonant EUV/x-ray probing can unlock the possibility of detecting the ultrafast electronic response at the nanoscale. Signatures of an ultrafast electron-lattice relaxation dynamics were indeed reported contextually to the demonstration of transient magnetic gratings driven by EUV TGs [9]. Electron-lattice relaxation dynamics were also reported in EUV TG experiments with optical probes [5,13,14], and indications about the influence of the Auger mechanism were inferred [15]; however, all these studies are inherently unable to access sub-100 nm length scales because of the long wavelength of the optical probe. In a broader perspective, the capability of driving and detecting electronic dynamics with multiple EUV pulses may enable nanoscale four-wave mixing studies of electronic correlations and dynamics with element and chemical-state sensitivity. The feasibility of such studies was theoretically evaluated in great detail, and the resulting perspectives represent an important motivation for developing four-wave mixing and other nonlinear optical approaches in the EUV and x-ray ranges [16–18].

In this manuscript, we report on a study focused on detecting ultrafast electronic dynamics in nanoscale EUV TG experiments on an elemental sample (Co), to showcase the feasibility of this kind of study. The manuscript is organized as follow: The experimental details and examples of EUV TG data are provided in Sec. II, Sec. III describes the data analysis,

*Contact author: filippo.bencivenga@elettra.eu

Published by the American Physical Society under the terms of the Creative Commons Attribution 4.0 International license. Further distribution of this work must maintain attribution to the author(s) and the published article's title, journal citation, and DOI.

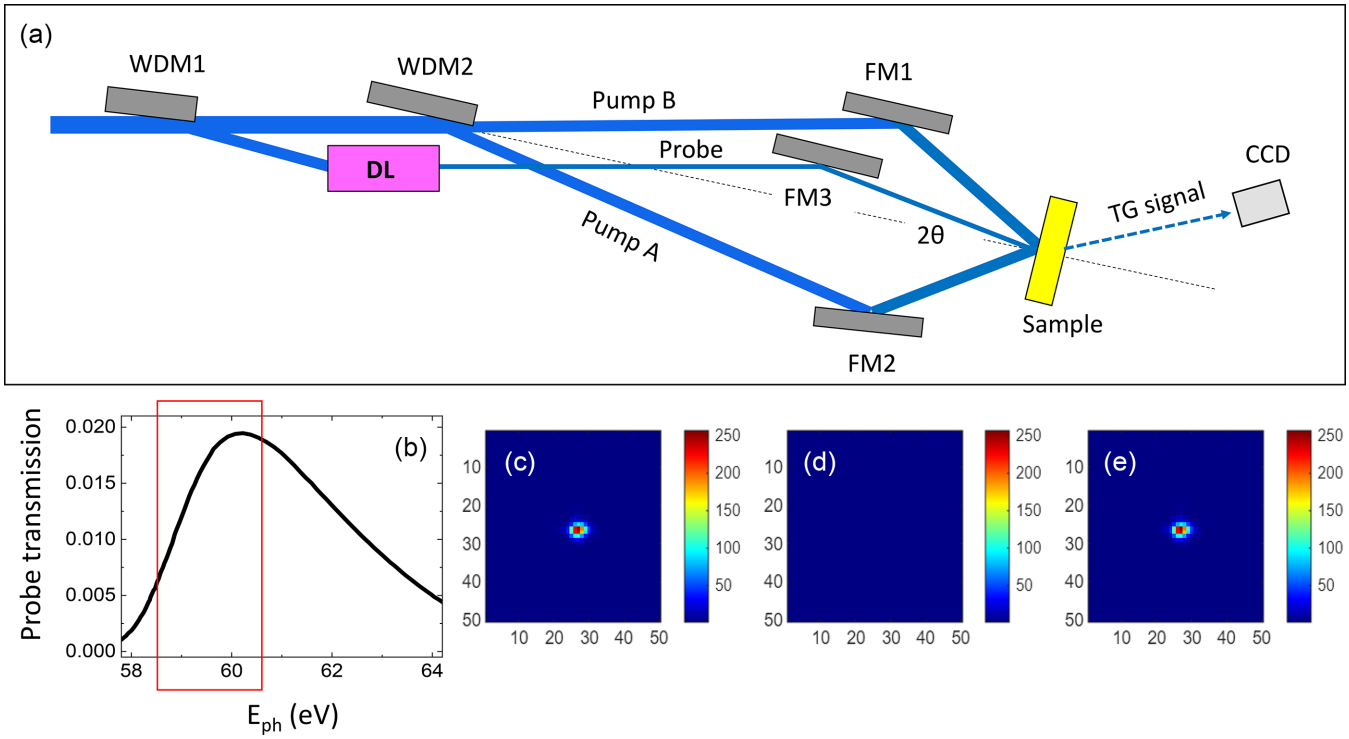


FIG. 1. (a) Sketch of the TG experiment. WDM1 and WDM2 are wavefront division plane mirrors, FM1, FM2, and FM3 are the focusing mirrors of the pump B, pump A and probe beams, respectively, while DL is the delay-line system. The dashed arrow sketches the EUV TG signal, which is detected by a CCD camera. (b) Transmission of the probe's branch line, including all elements from the source to the sample; the red rectangle indicates the E_{ph} range used here. (c) and (d) display CCD images with pump ON and pump OFF, respectively, while the difference between the two images is shown in (e); all images were collected for $t = 0.3$ ps.

Sec. IV reports a short discussion, and Sec. V presents the conclusions.

II. EXPERIMENT

Figure 1(a) sketches the experiment, which was performed at the TIMER instrument of the FERMI free-electron laser (FEL). The TIMER setup was used to split the FEL pulse into three, by means of wavefront division mirrors. Two of them (pump) are focused at the sample in time coincidence and with a crossing angle $2\theta = 27.6^\circ$, generating an EUV TG with period $L_{TG} = \lambda/2\sin(\theta)$, with λ the wavelength of the crossed pulses. The third pulse (probe) is time delayed by a EUV delay line based on four right-angle multilayer (ML) mirrors and is focused at the sample with an angle of incidence $\theta_p = 4.5^\circ$ (with respect to the sample's surface normal, which is oriented parallel to the bisector of the pump beams). The use of ML mirrors makes the transmission of the probe pulse through the TIMER instrument dependent on the photon energy (E_{ph}), as shown in Fig. 1(b). The transmission of the two pump pulses through the TIMER instrument was instead constant in the narrow range in E_{ph} used in the present work and approximately equal to 0.05. Further details on the instrument can be found elsewhere [19].

The sample was a Co film of thickness $d = 20$ nm, deposited on a 30 nm thick Si_3N_4 membrane. No capping layer was present; therefore, the surface was likely oxidized. Table I reports the relevant physical parameters for both Co and Si_3N_4. In the present experiment, the value of E_{ph} was the same for pump and probe, and it was varied in the 58.5–60.5 eV range, i.e., around the $M_{2,3}$ core-hole resonance of Co ($E = 59.6$ eV), resulting in a 44.4–43 nm range in L_{TG}. This small variation in L_{TG} is not expected to provide relevant changes in the ultrafast electronic response, eventual changes can thus be ascribed to resonant effects. The estimated time duration of the FEL pulses was 60 fs full width at half maximum (FWHM), and the repetition rate was 50 Hz. The spot size of the pump and probe pulses was about 300 and 200 μm FWHM, the pump fluence at the sample was in the 3–8 mJ/cm^2 range (within a FWHM), and hints of sample damage were not observed. Data were collected in transmission geometry by a CCD camera placed after the sample; see Fig. 1(a). The signal image was obtained by subtracting the pump OFF image from the pump ON one, as shown in Figs. 1(c)–1(e). The EUV TG signal intensity [$I_{TG}(t)$] was

TABLE I. Physical quantities of the materials present in the sample. For the absorption length, we report the values at the extrema of the exploited E_{ph} range, i.e., 58.5 and 60.5 eV. The values of density and sound velocity refer to bulk samples; for thin film the actual values may deviate.

	Si_3N_4	Co
Density (g/cm^3)	3.2 [20]	8.9
Longitudinal sound velocity (km/s)	9.2 [20]	5.8 [21]
Absorption length (nm)	14.3–9.7 [22]	50–52 [22]

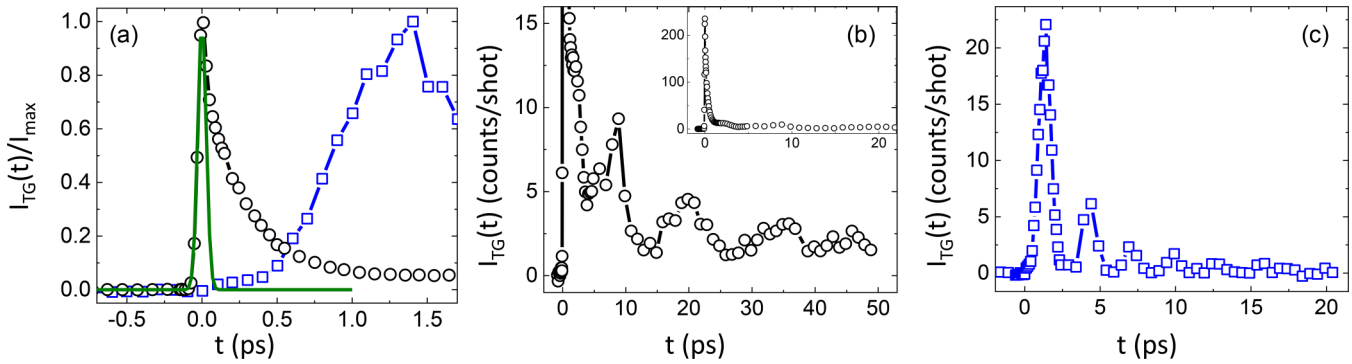


FIG. 2. (a) Resonant (black circles connected by lines) and nonresonant (blue squares connected by lines) EUV TG data from Co, normalized to amplitude of the maximum signal. The green line is a Gaussian centered at $t = 0$ and with a FWHM of 90 fs. Not normalized signals are reported in (b) and (c) in an extended range in t and using the same color code. The vertical scale in (b) was narrowed to show the thermoelastic response, data in the full vertical scale are displayed is the inset.

then obtained by integrating a small region of interest around the diffraction spot. Non-resonant data were collected from the same sample but in a separate experimental run, here we used distinct photon energies for the pump (46.6 eV) and the probe (93.2 eV), the value of 2θ was also different and yielded $L_{TG} = 16.7$ nm.

The $I_{TG}(t)$ waveform acquired by using a resonant (black circles; average of three scans) and nonresonant probe (blue squares; average of two scans) is displayed in Fig. 2(a) in a narrow time delay range around time zero. Data are normalized to the respective maximum signal intensity (I_{max}) and compared with a Gaussian function centered at $t = 0$ and with an FWHM of 90 fs, which is a reasonable approximation of the resolution function. Resonant EUV TG data ($E_{ph} =$ 59.6 eV) are featured by a sharp peak at $t = 0$, with a Gaussian rise time compatible with a resolution-limited response of 90 fs FWHM, followed by a few 100s of fs exponential decay, which is the characteristic timescale for the relaxation of the electronic population grating into lattice heating via electron-phonon coupling [5,23–26]. Faster dynamics involving excited electrons, such as the thermalization of the electronic gas, fall outside the time resolution of the present experiment. Conversely, no signal at $t = 0$ is observed in nonresonant data, here the maximum signal is achieved after half of the acoustic period, as expected from a purely thermoelastic response [4,7,8]. This comparison highlights the possibility of detecting the ultrafast electronic response by tuning E_{ph} to a core-hole resonance, which was one of the aims of this experiment.

Figures 2(b) and 2(c) show the signal without normalization and in an extended time delay range. It is worth stressing that the count rate in Figs. 2(b) and 2(c) cannot be compared with each other, because of the different experimental conditions, therefore, the following considerations are limited to the shape of the individual waveforms. Both the resonant and nonresonant signals are featured by the typical thermoelastic response, consisting of oscillations due to phonon propagation and a slower decay due to the relaxation of the thermal grating [7]. Note that the resonant signal is plotted in a restricted vertical scale in the main panel of Fig. 2(b), the full vertical scale is shown in the inset in order to highlight the about 50 times larger signal intensity of the electronic response with respect to the thermoelastic one.

Additional resonant EUV TG data were collected as a function of E_{ph} in a restricted time delay range, due to the limited amount of available beamtime.

III. DATA ANALYSIS

I_{TG}(t) is proportional to the square of the time-dependent variations of the complex refractive index at the probe's wavelength ($|\Delta n(t)|^2$) [5,7]. The thermoelastic dynamics is initialized by the relaxation of the electronic population grating into lattice heating, resulting in a lattice temperature grating which, through thermal expansion, triggers a density grating. This process results in refractive index variations, and any probe's wavelength, since the EUV refractive index is linearly proportional to density [27]. The electronic population grating excited by the EUV TG also alters the refractive index, but such changes are expected to be tangible only when the photon energy of the EUV probe is tuned to an electronic resonance of an atomic species present in the material; this actually provides element selectivity.

Since the EUV TG signal is measured by an intensity detector, the field amplitudes of the electronic [$S_{el}(t)$] and the thermoelastic signal [$S_{TE}(t)$] coherently add

$$I_{TG}(t) = R(t) \otimes [S_{el}(t) + S_{TE}(t)]^2, \quad (1)$$

where $\otimes$ is the convolution operator, and $R(t)$ is the instrumental resolution, which we assumed to have a Gaussian shape. Both $S_{TE}(t)$ and $S_{el}(t)$ are zero for $t < 0$, because no diffraction occurs before the arrival of the EUV TG pump (see Fig. 2).

$S_{TE}(t)$ accounts for thermoelastic dynamics, which decays via heat transport (the latter is responsible for the signal decay at long timescales) and is modulated by acoustic oscillations:

$$S_{TE}(t) = A_{th}e^{-t/\tau_{th}} - \Sigma_i A_i e^{-t/\tau_i} cos(2\pi \nu_i t), \quad (2)$$

where A_i and A_{th} are time-independent amplitudes, τ_i and τ_{th} are, respectively, the decay time of ith phonon mode and of the thermal grating, are ν_i are the acoustic frequencies [7,8,28]. Although the study of the thermoelastic response is not the main subject of the present work, we briefly analyzed also the full EUV TG waveform. In order to identify the acoustic frequencies, we first fitted the data to Eqs. (1) and (2) with

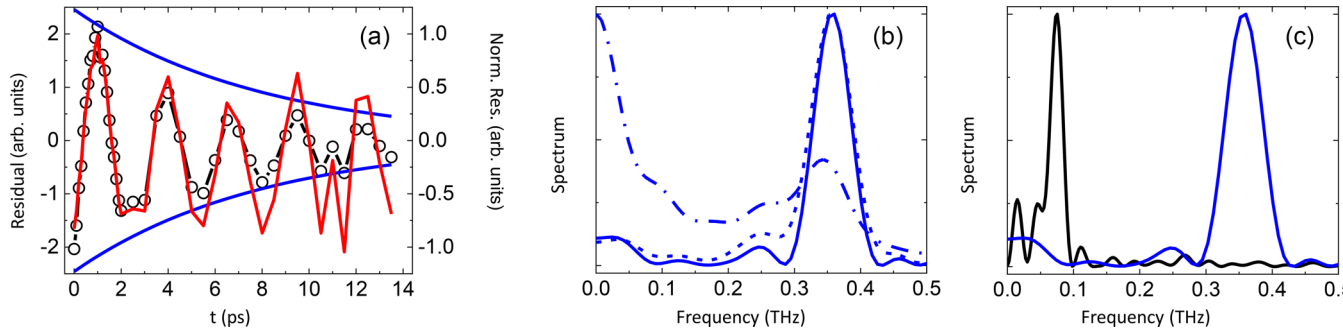


FIG. 3. (a) Black dots connected by lines (left vertical scale) are the residual EUV TG waveform, i.e., the square root of the raw data after subtraction of the thermal decay, for the nonresonant pump dataset, while the blue lines are the $\pm e^{-t/\tau_1}$ time decay. Red line (right vertical scale) is the residual normalized by the decay. (b) Fourier transform of the latter dataset (full line), of the residual (dashed line) and of the raw waveform (dash-dotted line). (c) The blue line is the same as in panel b, while the black line is the Fourier transform of the normalized residual for the resonant EUV TG data.

$i = 1$ and $S_{\rm el} = 0$, in order to estimate the main parameters of the thermoelastic waveform. We subtracted the thermal decay ($A_{th}e^{-t/\tau_{th}}$), as obtained by the fit, from the square root of the raw data, scaled the result of the subtraction by e^{-t/τ_1} and performed a Fourier transform. Figures 3(a) and 3(b) illustrate this procedure in the case of the nonresonant pump (dataset in blue in Fig. 2), while Fig. 3(c) shows the Fourier spectrum of the waveforms displayed in Figs. 2. The frequency of the main acoustic mode fairly scales with $L_{\rm TG}$ and in the case of the nonresonant waveform (where $d/L_{\rm TG} \approx 1$), is consistent with a propagation velocity ($c = \nu L_{\rm TG} \approx 5.9$ km/s) matching literature values [29]. For the longer TG period (resonant waveform), the condition $d/L_{\rm TG} < 1$ is meet. In this case, the acoustic dispersion is no longer linear, and it consists in multiple modes, called Lamb waves, whose amplitude generally increases on decreasing the $d/L_{\rm TG}$ ratio and is larger for the modes with phase velocity closer to the longitudinal and transverse velocity [30–32]. A second weaker mode can be supposed at a lower frequency and can be likely ascribed to a Lamb mode.

The main dataset consists in additional resonant EUV TG data as a function of $E_{\rm ph}$ (single scans), collected in a narrower time delay range (≈1 ps) around the electronic peak. In such a narrow range, $S_{\rm TE}(t)$ can be approximated by a constant (and almost negligible) offset, while we empirically assumed that the electronic response can be described as

$$S_{el}(t) = A_0\delta(t) + A_{el}e^{-t/\tau_{el}}, \quad (3)$$

where $A_{\rm el}$ and τ_{el} are the amplitude and characteristic time of the observed ultrafast decay, respectively, while $A_0\delta(t)$ is an "instantaneous" term accounting for any response much faster than our time resolution. The time dependence of the experimental signal in the 1 ps time delay range was thus approximated by

$$I_{TG}(t) = A_0^2 R(t) + \frac{1 + \mathrm{erf}(t/\sigma)}{2}[A_{el}e^{-t/\tau_{el}} + A_{TE}]^2, \quad (4)$$

where $A_{\rm TE}$ is the aforementioned offset, while the factor $(1 + \mathrm{erf}(t/\sigma))/2$, with 2.355σ the FWHM of $R(t)$, approximates the convolution with the instrumental response and accounts for the null values of $S_{\rm TE}(t)$ and $S_{\rm el}(t)$ at $t < 0$. This simplified model function well describes the experimental data, as shown in Fig. 4. On inspecting this figure, one can appreciate the "kink" located just below 100 fs time delay, due to the presence of an instantaneous electronic response [i.e., the $A_0\delta(t)$ term] on top of the exponential decay of the electronic population grating, as well as the shorter decay time at the lower value of $E_{\rm ph}$.

IV. DISCUSSION

Figure 5 shows the trend of the parameters featuring the ultrafast electronic response, i.e., $\tau_{\rm el}$, $A_{\rm el}$ and A_0, as a function of $E_{\rm ph}$. The trend of the $A_0/A_{\rm el}$ ratio as a function of $E_{\rm ph}$ is displayed in Fig. 5(a), it is almost constant in the probed range, within the error bars, even if a minimum roughly in correspondence of the resonant energy can be supposed. A constant ratio indicates that eventual dynamical processes faster than our time resolution have the same dependencies on $E_{\rm ph}$ as the decay dynamics of the electronic population grating, which is quite reasonable, since faster processes must also have an electronic origin. It is worth mentioning that the $A_0\delta(t)$ term may be due to a "coherent spike" [33,34]; a more detailed account for this will be presented in a following report. Indeed, at $t = 0$ the TG formed by one of the pump and the probe can diffract the other pump. In the employed geometry, the diffraction angle of the pump A off the grating formed by the pump B and the probe [see Fig. 1(a) for the beam labelling] is exactly the same as the one of the probe diffracted off the TG formed by pump A and pump B. However, the time delay has a different meaning for the two processes: for the diffraction of the probe off the grating formed by the two pump, it is a regular pump-probe delay, while for the coherent spike signal (diffraction of the pump A off the grating formed by the pump B and the probe) the same delay controls the TG amplitude and the pump A that acts as a time-zero probe. Since a coherent spike also originates from an electronic response, a constant $A_0/A_{\rm el}$ ratio is indeed expected. A different experimental geometry can spatially discriminate the regular EUV TG (pump-probe) signal from the coherent spike.

Figure 5(b) displays the almost constant values of the FWHM of the erf function describing the time resolution, as obtained from the fit, and the time decay of the electronic

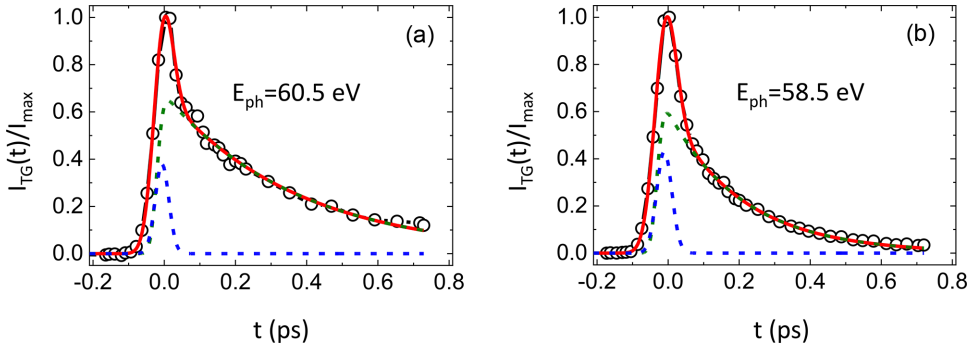


FIG. 4. Resonant (black circles connected by lines) EUV TG waveforms at the indicated values of E_{ph}. The red lines are the best-fit results, while the blue and green dashed lines are the separate contributions of the "instantaneous" response and the ultrafast decay, respectively.

population grating (τ_{el}), which increases with E_{ph} by a factor $\approx$2 up to reach the resonant energy, while the value of τ_{el} at the larger photon energy (above resonance) seems to decrease. The three data points at 59.6 eV correspond to EUV TG data collected before, during and after the dataset as a function of E_{ph}. The consistency between these data suggest a reasonable reproducibility. Unfortunately, the dataset is too limited and error bars are too large for suggesting the presence of resonant effects, in addition, the dependence of τ_{el} on E_{ph} could be affected by the increasing density of excitation photons. Indeed, the experiment was not performed at constant fluence, and the absorption length (L_{abs}) of Co substantially changes in the probed E_{ph} range, decreasing from 14.5 nm at $E_{ph} = 58.5$ eV to 9.5 nm at $E_{ph} = 60.5$ eV [22]. As the penetration depth decreases, the observed time decay increases, suggesting a dependence on the absorbed energy density. In addition, not constant values of L_{abs} could reflect into non-negligible effects due to electron-lattice thermalization along the film thickness, not only within the interaction volume. We finally mention that the thickness of the sample (20 nm) is not much larger than L_{abs}, therefore, the Si_3N_4 membrane can be slightly photoexcited. We can, however, exclude that a fraction of the signal comes from Si_3N_4, because of the largely off-resonant conditions.

Figure 6 displays the trend of τ_{el} as a function of the number of photons per atom absorbed in the sample (N), estimated as $N = 2F(1 - e^{-d/L_{abs}})/d\rho$, where F is the excitation fluence in photons per unit area, and ρ is the number density, while the factor 2 accounts for the fact that in the EUV TG fringes the energy density is twice the average value. This estimate is very crude, since it assumes that all ballistic electrons that initialize the electron-phonon coupling do not escape the interaction region (e.g., by photoemission), and it completely neglects surface oxidation. Such a range in N corresponds to an excitation energy density of a few kJ/cm^3, which is far from the energy density regime, where strong and exotic dependencies of τ_{el} on the excitation energy could be supposed. Based on previous results on ultrafast electronic relaxations in laser-excited metals, disregarding EUV core-resonance effects (it is worth stressing that these works deal with optical laser excitation), one may expect a decrease in τ_{el} with N [23,35,36]. Conversely, data in Fig. 6 do not show this trend, in addition, data points at different values of E_{ph} but at the same value of N are featured by different relaxation times. This evidence suggests that N is a variable that does not correlate well with τ_{el}. A possible explanation could be that resonance effects due to core-excitation dynamics (such as the Auger mechanisms) alter the response of the electronic system and its thermalization with the lattice, as reported in a previous EUV TG experiment with optical probe [15]. However, further studies as a function of E_{ph} for given values of N, with possibly a substantially better time resolution for resolving faster electron dynamics, are needed to properly investigate such nanoscale electron-lattice relaxation dynamics.

A more extended experimental campaign could allow us to determine the electronic response as a function of the

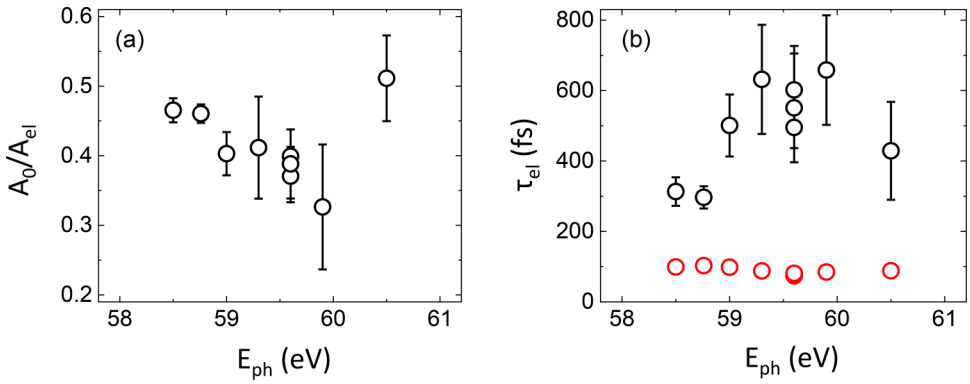


FIG. 5. (a) Ratio between A_0 and A_{el} as a function of E_{ph}. (b) Black circles are best fit values of τ_{el} as a function of E_{ph}, red circles is the FWHM of the erf function [see Eq. (2)]; in the latter dataset, the error bars are smaller than the size of the dots.

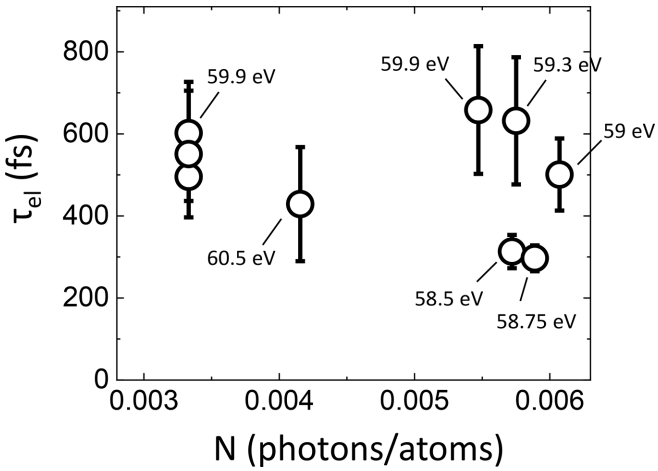


FIG. 6. Best fit values of τ_{el} as a function of the estimated value of N. The labels identify the values of E_{ph}.

excitation fluence at each given value of photon energy (or vice versa), hence decoupling the dependencies on E_{ph} and N and likely providing additional information about resonance effects. The latter might also include coherent EUV four-wave-mixing processes. A larger range in both N and E_{ph} can also help us in better characterizing the trend of τ_{el}. Unfortunately, the limited amount of beamtime prevented us to extend this study to larger values of E_{ph}; note that values up to about 64 eV are possible with the present setup [see Fig. 1(b)].

V. CONCLUSIONS AND OUTLOOKS

In conclusion, the present experimental study demonstrates the possibility of using resonant EUV TG to determine the ultrafast electron-lattice relaxation dynamics. The experiments hereby reported were carried out on a Co thin film with a likely oxidized surface, by exploiting the $M_{2,3}$ core-hole resonance, located at about 59.6 eV. However, we expect that this type of study can be carried out in any material, provided that the EUV probe is tuned to a proper core-hole resonance. This kind of experiment can complement resonant EUV self-diffraction studies [37], carried out at the same instrument, where the photon energy dependence of the EUV TG signal at time zero is detected, without technical restrictions in the exploitable photon energy range.

We observed that the dynamics of the electronic population grating induced by the pump is not detectable in nonresonant conditions and the only appreciable signal is due to the thermoelastic response, which extends over the 10s of ps timescale and has an almost null signal at time zero. In resonant conditions, a sharp time-zero peak with amplitude much larger than the thermoelastic response is observed. Such a peak shows a resolution-limited risetime and a 100s fs decay time, reflecting the ultrafast relaxation of the electronic population grating into lattice excitations. The dependence of the electronic response was studied as a function of the photon energy in a narrow range (limited by experimental constraints) close to the $M_{2,3}$ edge. We observed that the time decay of the electronic population grating slows down when the photon energy is increased from below to above the $M_{2,3}$ edge. Data suggest that such a slowing down is not related to changes in the excitation energy density. However, additional studies are needed in order to confirm such indications and for decoupling eventual effects due to the EUV resonance from effects due to the excitation energy density. We also found signatures of a response faster than the time resolution, whose amplitude is proportional to that of the electronic grating,- and it may be due to a timezero coherent spike.

This initial study represents a step towards the experimental handling of the ultrafast electronic four-wave-mixing response, highlighting the reliability of the EUV TG approach in this context. Indeed, the use of an EUV TG excitation instead of a conventional pump permits to impose a nanoscale spatial modulation, which can in be, in principle, tuned to values as short as some nm. This could represent a relevant parameter to add nanoscale sensitivity to electronic dynamics studies. Besides extending these studies to other samples and absorption edges, as well as studies as a function of the excitation energy density, other specific outlooks can be envisioned: (i) in the present experiment, the photon energy of the excitation and probe beams was the same, preventing us to distinguish resonant effects due to the excitation and probe processes. This limitation can be easily removed by using two-color FEL pulses, which are available at FELs and normally used in EUV TG experiments. (ii) The time resolution is limited to about 100 fs not only by the FEL pulse duration but also by the quite large footprint and wavefront tilt of the beams, hence limiting the experimental capabilities to the relatively slow dynamics of the electronic population grating. The use of shorter FEL pulses (already demonstrated in many FEL facilities), as well as smaller focal spots and crossing angles, can greatly mitigate this limitation, potentially enabling the study of purely electronic dynamics, such as the thermalization of hot electron gas or core-hole recombination. The photon energy range of the probe is also instrumentally limited. Different approaches, such as the use of diffractive optics, can reduce such limitations [38]. (iii) EUV TG in reflection geometry can be used to determine electronic dynamics at the surface. Indeed, time-dependent variations of the refractive index at the surface [$\Delta n_s(t)$] result in a spatial modulation of the reflectivity of the EUV probe, which can lead to a transient diffraction signal in reflection [5]. Preliminary measurements indicate that this signal is detectable but the present sample is of insufficient quality in terms of surface roughness and oxygen contamination; a more detailed study on a better sample will likely be carried out in the near future. (iv) Since the capability of realizing x-ray TGs was demonstrated [39], also with the use of x-ray probes [40], the extension of these studies at x-ray photon energies is a reasonable perspective and would enable us to substantially enlarge the range of exploitable core-hole resonances.

ACKNOWLEDGMENTS

This work was supported in part by the Italian Ministry of Foreign Affairs and International Cooperation under Grant No. PGR12339-XSIM.

DATA AVAILABILITY

The data that support the findings of this article are openly available [41].

[1] Q. Li, K. Hoogeboom-Pot, D. Nardi, M. M. Murnane, H. C. Kapteyn, M. E. Siemens, E. H. Anderson, O. Hellwig, E. Dobisz, B. Gurney, *et al.*, Generation and control of ultrashort-wavelength two-dimensional surface acoustic waves at nanoscale interfaces, Phys. Rev. B **85**, 195431 (2012).

[2] T. D. Frazer, J. L. Knobloch, J. N. Hernández-Charpak, K. M. Hoogeboom-Pot, D. Nardi, S. Yazdi, W. Chao, E. H. Anderson, M. K. Tripp, S. W. King, *et al.*, Full characterization of ultrathin 5-nm low- k dielectric bilayers: Influence of dopants and surfaces on the mechanical properties, Phys. Rev. Mater. **4**, 073603 (2020).

[3] M. E. Siemens, Q. Li, R. Yang, K. A. Nelson, E. H. Anderson, M. M. Murnane, and H. C. Kapteyn, Quasi-ballistic thermal transport from nanoscale interfaces observed using ultrafast coherent soft X-ray beams, Nat. Mater. **9**, 26 (2010).

[4] F. Bencivenga, R. Mincigrucci, F. Capotondi, L. Foglia, D. Naumenko, A. A. Maznev, E. Pedersoli, A. Simoncig, F. Caporaletti, V. Chiloyan, *et al.*, Nanoscale transient gratings excited and probed by extreme ultraviolet femtosecond pulses, Sci. Adv. **5**, eaaw5805 (2019).

[5] F. Bencivenga, F. Capotondi, L. Foglia, R. Mincigrucci, and C. Masciovecchio, Extreme ultraviolet transient gratings, Adv. Phys. X **8**, 2220363 (2023).

[6] F. Bencivenga and C. Masciovecchio, FEL-based transient grating spectroscopy to investigate nanoscale dynamics, Nucl. Instrum. Methods. Phys. Res. A **606**, 785 (2009).

[7] L. Foglia, R. Mincigrucci, A. A. Maznev, G. Baldi, F. Capotondi, F. Caporaletti, R. Comin, D. De Angelis, R. A. Duncan, D. Fainozzi, *et al.*, Extreme ultraviolet transient gratings: A tool for nanoscale photoacoustics, Photoacoustics **29**, 100453 (2023).

[8] A. A. Maznev, R. Mincigrucci, F. Bencivenga, V. Unikandanunni, F. Capotondi, G. Chen, Z. Ding, R. A. Duncan, L. Foglia, M. G. Izzo, *et al.*, Generation and detection of 50 GHz surface acoustic waves by extreme ultraviolet pulses, Appl. Phys. Lett. **119**, 044102 (2021).

[9] D. Ksenzov, A. A. Maznev, V. Unikandanunni, F. Bencivenga, F. Capotondi, A. Caretta, L. Foglia, M. Malvestuto, C. Masciovecchio, R. Mincigrucci, *et al.*, Nanoscale transient magnetization gratings created and probed by femtosecond extreme ultraviolet pulses, Nano Lett. **21**, 2905 (2021).

[10] K. Yao, F. Steinbach, M. Borchert, D. Schick, D. Engel, F. Bencivenga, R. Mincigrucci, L. Foglia, E. Pedersoli, D. De Angelis, *et al.*, All-optical switching on the nanometer scale excited and probed with femtosecond extreme ultraviolet pulses, Nano Lett. **22**, 4452 (2022).

[11] F. Steinbach, U. Atxitia, K. Yao, M. Borchert, D. Engel, F. Bencivenga, L. Foglia, R. Mincigrucci, E. Pedersoli, D. De Angelis, *et al.*, Exploring the fundamental spatial limits of magnetic all-optical switching, Nano Lett. **24**, 6865 (2024).

[12] P. R. Miedaner, N. Berndt, J. Deschamps, S. Urazhdin, N. Khatu, D. Fainozzi, M. Brioschi, P. Carrara, R. Cucini, G. Rossi, *et al.*, Excitation and detection of coherent nanoscale spin waves via extreme ultraviolet transient gratings, Sci. Adv. **10**, eadp6015 (2024).

[13] F. Bencivenga, A. Calvi, F. Capotondi, R. Cucini, R. Mincigrucci, A. Simoncig, M. Manfredda, E. Pedersoli, E. Principi, F. Dallari, *et al.*, Four-wave-mixing experiments with seeded free electron lasers, Farad. Discuss. **194**, 283 (2016).

[14] F. Bencivenga, R. Cucini, F. Capotondi, A. Battistoni, R. Mincigrucci, E. Giangrisostomi, A. Gessini, M. Manfredda, I. P. Nikolov, E. Pedersoli, *et al.*, Four-wave mixing experiments with extreme ultraviolet transient gratings, Nature (London) **520**, 205 (2015).

[15] R. Bohinc, G. Pamfilidis, J. Rehault, P. Radi, C. Milne, J. Szlachetko, F. Bencivenga, F. Capotondi, R. Cucini, L. Foglia, *et al.*, Nonlinear XUV-optical transient grating spectroscopy at the Si $L_{2,3}$–edge, Appl. Phys. Lett. **114**, 181101 (2019).

[16] S. Tanaka and S. Mukamel, Coherent x-ray raman spectroscopy: A nonlinear local probe for electronic excitations, Phys. Rev. Lett. **89**, 043001 (2002).

[17] S. Mukamel, Multiple core-hole coherence in x-ray four-wave-mixing spectroscopies, Phys. Rev. B **72**, 235110 (2005).

[18] S. Mukamel, D. Healion, Y. Zhang, and J. D. Biggs, Multidimensional attosecond resonant x-ray spectroscopy of molecules: Lessons from the optical regime, Annu. Rev. Phys. Chem. **64**, 101 (2013).

[19] R. Mincigrucci, L. Foglia, D. Naumenko, E. Pedersoli, A. Simoncig, R. Cucini, A. Gessini, M. Kiskinova, G. Kurdi, N. Mahne, *et al.*, Advances in instrumentation for FEL-based four-wave-mixing experiments, Nucl. Instrum. Methods. Phys. Res. A **907**, 132 (2018).

[20] R. C. Brown and P. K. Swaminathan, Silicon nitride equation of state, AIP Conf. Proc. **1793**, 050013 (2017).

[21] D. Antonangeli, M. Krisch, G. Fiquet, J. Badro, D. L. Farber, A. Bossak, and S. Merkel, Aggregate and single-crystalline elasticity of hcp cobalt at high pressure, Phys. Rev. B **72**, 134303 (2005).

[22] CXRO - https://henke.lbl.gov/optical_constants/, (n.d.).

[23] B. Rethfeld, A. Kaiser, M. Vicanek, and G. Simon, Ultrafast dynamics of nonequilibrium electrons in metals under femtosecond laser irradiation, Phys. Rev. B **65**, 214303 (2002).

[24] B. Y. Mueller and B. Rethfeld, Relaxation dynamics in laser-excited metals under nonequilibrium conditions, Phys. Rev. B **87**, 035139 (2013).

[25] U. Ritzmann, P. M. Oppeneer, and P. Maldonado, Theory of out-of-equilibrium electron and phonon dynamics in metals after femtosecond laser excitation, Phys. Rev. B **102**, 214305 (2020).

[26] L. Waldecker, R. Bertoni, R. Ernstorfer, and J. Vorberger, Electron-phonon coupling and energy flow in a simple metal beyond the two-temperature approximation, Phys. Rev. X **6**, 021003 (2016).

[27] D. T. Attwood, *Soft X-Rays and Extreme Ultraviolet Radiation: Principles and Applications, 1. paperback version, digitally printed* (with amendments) (Cambridge University Press, Cambridge, 2007).

[28] K. A. Nelson and M. D. Fayer, Laser induced phonons: A probe of intermolecular interactions in molecular solids, J. Chem. Phys. **72**, 5202 (1980).

[29] V. V. Roshchupkin, M. M. Lyakhovitskii, M. A. Pokrasin, N. A. Minina, A. I. Chernov, N. L. Sobol, S. A. Klimenko, M. Yu. Kopeikina, and A. G. Koltsov, Investigation of the acoustic properties of cobalt, High Temp. **52**, 846 (2014).

[30] A. Milloch, R. Mincigrucci, F. Capotondi, D. De Angelis, L. Foglia, G. Kurdi, D. Naumenko, E. Pedersoli, J. S. Pelli-Cresi, A. Simoncig, *et al.*, Nanoscale thermoelasticity in silicon nitride membranes: Implications for thermal management, ACS Appl. Nano Mater. **4**, 10519 (2021).

[31] J. S. Meth, C. D. Marshall, and M. D. Fayer, Experimental and theoretical analysis of transient grating generation and detection of acoustic waveguide modes in ultrathin solids, J. Appl. Phys. **67**, 3362 (1990).

[32] J. A. Rogers and K. A. Nelson, Study of Lamb acoustic waveguide modes in unsupported polyimide thin films using real-time impulsive stimulated thermal scattering, J. Appl. Phys. **75**, 1534 (1994).

[33] H. J. Eichler, U. Klein, and D. Langhans, Coherence time measurement of picosecond pulses by a light-induced grating method, Appl. Phys. **21**, 215 (1980).

[34] W. L. Nighan, T. Gong, L. Liou, and P. M. Fauchet, Self-diffraction: A new method for characterization of ultrashort laser pulses, Optics Commun. **69**, 339 (1989).

[35] E. G. Gamaly and A. V. Rode, Electron–phonon energy relaxation in bismuth excited by ultrashort laser pulse: Temperature and fluence dependence, Appl. Phys. A **110**, 529 (2013).

[36] H. E. Elsayed-Ali, T. B. Norris, M. A. Pessot, and G. A. Mourou, Time-resolved observation of electron-phonon relaxation in copper, Phys. Rev. Lett. **58**, 1212 (1987).

[37] A. A. Maznev, W. Lee, S. K. Cushing, D. De Angelis, D. Fainozzi, L. Foglia, C. Gutt, N. Jaouen, F. Kammerbauer, C. Masciovecchio, *et al.*, Resonant Self-Diffraction of Femtosecond Extreme Ultraviolet Pulses in Cobalt, arXiv:2505.07168v1.

[38] L. Foglia, R. Mincigrucci, F. Doring, D. Fainozzi, T. Mamyrbayev, C. Masciovecchio, and F. Bencivenga, A new framework for soft x-ray transient gratings, J. Phys. B At. Mol. Opt. Phys. **57**, 145601 (2024).

[39] J. R. Rouxel, D. Fainozzi, R. Mankowsky, B. Rösner, G. Seniutinas, R. Mincigrucci, S. Catalini, L. Foglia, R. Cucini, F. Döring, *et al.*, Hard X-ray transient grating spectroscopy on bismuth germanate, Nat. Photon. **15**, 499 (2021).

[40] H. Li, N. Wang, L. Zhang, S. Song, Y. Sun, M.-L. Ng, T. Sato, D. Hanlon, S. Dahal, M. D. Balcazar, *et al.*, Nanoscale ultrafast lattice modulation with hard x-ray free electron laser, Nat. Phys. **22**, 483 (2026).

[41] Data are available here: https://doi.org/10.34965/enodo.i61100, https://doi.org/10.34965/enodo.i61101 and https://doi.org/10.34965/enodo.i61102.